DALTON

Dynamic stereochemical rearrangements in 'chiral-at-ligand' complexes. Tricarbonylhalogenorhenium(I) and halogenotrimethylplatinum(IV) complexes of 2,6-bis[4-(*S*)-methyloxazolin-2-yl]pyridine

Peter J. Heard* and Cameron Jones

Department of Chemistry, University of Wales, Swansea SA2 8PP, UK

Enantiomerically pure 2,6-bis[4-(*S*)-methyloxazolin-2-yl]pyridine, L, reacted with the pentacarbonylhalogenorhenium(I) and halogenotrimethylplatinum(IV) metal moieties to afford complexes of general formulae *fac*-[ReX(CO)$_3$L] and *fac*-[PtXMe$_3$L] (X = Cl, Br or I) in moderate yield. The potentially terdentate ligand acts here in a bidentate bonding mode, and undergoes a dynamic structural rearrangement which exchanges the pendant and co-ordinated oxazole rings. The bidentate bonding mode and absolute configuration of the ligand were confirmed by the crystal structure of the complex [ReCl(CO)$_3$L]. The chiral centres on the ligand provide an excellent spectroscopic handle on the mechanism of the rearrangement, and two independent fluxional pathways are apparent. The energetics of the rearrangement in the complexes [ReX(CO)$_3$L] (X = Cl, Br or I) was measured by standard ^{1}H NMR band-shape analysis; $\Delta G^{\ddagger}$(average) (298 K) is 74.3 kJ mol^{-1} for the 'tick-tock twist' mechanism and 84.0 kJ mol^{-1} for the 'rotation' mechanism. Platinum-195 NMR data are reported for the complexes [PtXMe$_3$L] (X = Cl, Br or I).

In the transition-metal complexes of 2,2′:6′,2″-terpyridine (terpy) reported hitherto the ligand usually exhibits a terdentate bonding mode.[1] However, if the bonding is somehow restricted to a bidentate mode the resultant complexes are fluxional; an exchange occurs between the pendant and co-ordinated (outer) pyridyl rings.[2–7] Other potentially terdentate ligands also display fluxional behaviour when restricted to bidentate bonding modes; compounds investigated in this context are pyrazolylbipyridines,[8] bis(pyrazolyl)pyridines,[9] and mixed donors such as 2,6-bis(methylsulfanylmethyl)pyridine (S,N,S)[10,11] and bis[*o*-(methylsulfanyl)phenyl]phenylphosphine (S,P,S).[12,13]

Two possible mechanisms were initially proposed by Abel, Orrell and co-workers[2,10] for the dynamic structural rearrangements observed in the terpyridine (and related) complexes (Scheme 1). Subsequent analysis of the effect of the fluxional process on the NMR signals of the methylplatinum groups in the PtXMe$_3$ complexes of (terpy)[2] and 2,6-bis(methylsulfanylmethyl)pyridine[11] (X = Cl, Br or I), and the pentafluorophenyl rings in the complex *cis*-[Pd(C$_6$F$_5$)$_2$(terpy)],[6] indicated that the mechanism involved a 1,4-metallotropic shift, with the ligand adopting a pseudo-terdentate bonding mode in the transition state: the so called 'tick-tock twist' mechanism [(ii) in Scheme 1]. However, this mechanism has been the subject of some controversy. Rotondo *et al.*[7] examined the effect of acids on the rate of the fluxional rearrangement in *cis*-[M(C$_6$F$_5$)$_2$(terpy)] (M = Pd or Pt), and concluded that the rate-determining step probably involved cleavage of the outer pyridyl Pt–N bond to form a 'T-shaped' intermediate, in which the ligand is bound to the metal by the central pyridyl ring N-donor atom alone. Whilst this interpretation is supported, at least in part, by some kinetic studies on platinum(II) sulfide complexes, which indicate dissociative reaction pathways for a number of ligand-substitution processes,[14] more recent work has demonstrated that a dissociative pathway is not involved.[6b]

The compounds 2,6-bis[4-(*S*)-alkyloxazolin-2-yl]pyridine are readily prepared, with retention of stereochemistry, from pyridine-2,6-dicarbonyl dichloride and the appropriate enantiomerically pure α-amino alcohol.[15] Oxazoline-based compounds are of much current interest because of their use as chiral auxiliaries in transition-metal-mediated enantioselective transformations.[16] The presence of a chiral centre also provides an excellent spectroscopic handle for the elucidation of fluxional mechanistic pathways. This paper describes the dynamic stereochemical behaviour of the tricarbonylhalogenorhenium(I) and halogenotrimethylplatinum(IV) complexes of 2,6-bis[4-(*S*)-methyloxazolin-2-yl]pyridine (L), *viz*. *fac*-[ReX(CO)$_3$L] and *fac*-[PtXMe$_3$L] (X = Cl, Br or I).

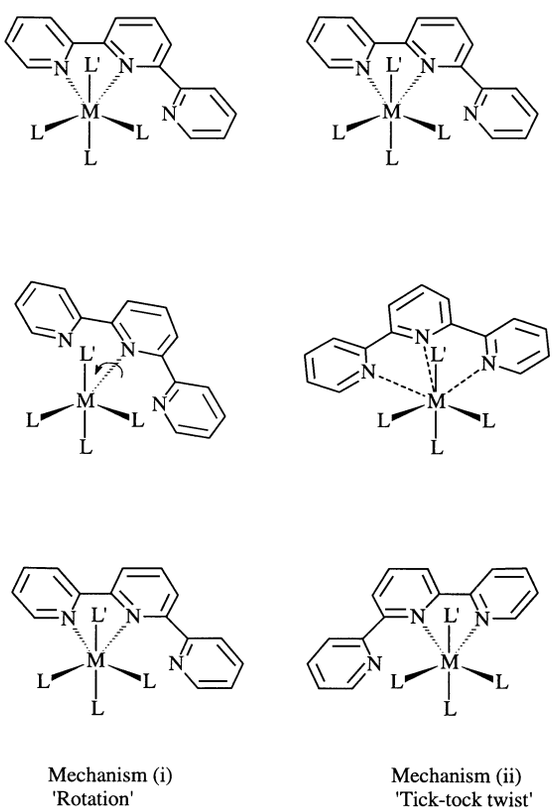

Scheme 1 The two mechanisms proposed by Abel *et al.* for the fluxional exchange in bidentate complexes of 2,2′:6′,2″-terpyridine

Experimental

Materials

The pentacarbonylhalogenorhenium(I)[17] and halogenotrimethylplatinum(IV)[18,19] compounds were prepared by previously published procedures. 2,6-Bis[4-(*S*)-methyloxazolin-2-yl]pyridine was prepared by the same procedure as that described[15] for 2,6-bis[4-(*S*)-isopropyloxazolin-2-yl]pyridine.

Synthesis of complexes

All manipulations were carried out under an atmosphere of dry, oxygen-free nitrogen using standard Schlenk techniques.[20] Solvents were dried[21] and degassed prior to use. The three rhenium complexes, $[ReX(CO)_3L]$ (X = Cl, Br or I), were prepared as illustrated by the example (X = I) given below. The three platinum complexes, $[PtXMe_3L]$ (X = Cl, Br or I), were prepared as illustrated by the synthesis of $[PtBrMe_3L]$. Analytical data for all six complexes are in Table 1.

{2,6-Bis[4-(*S*)-methyloxazolin-2-yl]pyridine}tricarbonyliodorhenium(I). Pentacarbonyliodorhenium(I) (0.12 g, 0.27 mmol) and 2,6-bis[4-(*S*)-methyloxazolin-2-yl]pyridine (0.10 g, 0.41 mmol) were refluxed for *ca.* 24 h in light petroleum (b.p. 60–80 °C)–benzene (2 : 1 v/v, 30 cm^3). The crude solid obtained was placed on a silica gel column, the column was washed with chloroform, then the product was eluted as an orange band using dichloromethane. The addition of hexane to the eluent gave 60 mg (35%) of crystalline, orange $[ReI(CO)_3L]$.

{2,6-Bis[4-(*S*)-methyloxazolin-2-yl]pyridine}bromotrimethylplatinum(IV). Bromotrimethylplatinum(IV) (0.10 g, 0.31 mmol based on the monomeric unit) and 2,6-bis[4-(*S*)-methyloxazolin-2-yl]pyridine (0.08 g, 0.33 mmol) were refluxed in benzene (10 cm^3) for *ca.* 5 h. The benzene was then removed *in vacuo* and the crude product dissolved in acetone. After filtration, hexane was added to the acetone solution to afford cream-white crystals of $[PtBrMe_3L]$ (70 mg, 42%).

Physical methods

Infrared spectra were recorded as CH_2Cl_2 solutions on a Perkin-Elmer 1725X Fourier-transform spectrometer, operating in the region 4000–400 cm^{-1}. Elemental analyses were carried out at the University of Wales, College of Cardiff. Fast atom bombardment (FAB) mass spectrometry was performed by Dr. J. A. Ballantine on a VG AutoSpec instrument, using Cs^+-ion bombardment at 25 kV energy. Hydrogen-1 NMR spectra were recorded as $(CDCl_2)_2$, $CDCl_3$ or CD_2Cl_2 solutions on a Bruker AC300 Fourier-transform spectrometer, operating at 300.13 MHz; chemical shifts are quoted relative to tetramethylsilane as an internal standard. Platinum-195 NMR spectra were obtained by Dr. V. Sik as $(CDCl_2)_2$ solutions on a Bruker DRX400 Fourier-transform spectrometer, operating at 85.80 MHz; chemical shifts are quoted relative to the absolute frequency scale, $\Xi(^{195}Pt) = 21.4$ MHz. The NMR spectrometer probe temperatures were controlled by a standard B-VT 2000 unit, which was periodically calibrated; probe temperatures are considered accurate to within ±1 °C. The band shapes of the variable-temperature ^1H NMR spectra were analysed using the DNMR 3 program.[22] Computer-simulated spectra were visually fitted with those obtained experimentally, and the 'best-fit' rate constants used to calculate the Eyring and Arrhenius activation parameters. The errors quoted are those defined by Binsch and Kessler.[23] Homonuclear (^1H–^1H) correlation spectra were obtained using the Bruker COSYPH program.[24]

Crystallography

Crystals of the complex $[ReCl(CO)_3L]$ were obtained by slow evaporation of a CH_2Cl_2 solution and transferred to the cold gas stream of the diffractomer.

Crystal data and data-collection parameters. $C_{16}H_{15}ClN_3O_5Re$, $M = 550.96$, $a = 11.1900(11)$, $b = 11.6830(8)$, $c = 13.676(2)$ Å, $U = 1787.9(3)$ $Å^3$, $T = 150(2)$ K, space group $P2_12_12_1$ (no. 19), Mo-Kα radiation, $\lambda = 0.71069$ Å, $Z = 4$, $D_c = 2.047$ Mg m^{-3}, $F(000) = 1056$, yellow block with dimensions 0.32 × 0.24 × 0.18 mm, $\mu = 6.979$ mm^{-1}, data collection range $2.29 < 2\theta < 25.07°$, 5934 reflections collected using a FAST TV area diffractometer,[25] giving 2736 unique ($R_{int} = 0.071$).

Structure solution and refinement. The structure was solved by heavy-atom methods using the SHELXL 86 program[26] and refined by full-matrix least squares on F^2, using SHELXL 93.[27] Neutral-atom complex scattering factors were employed.[28] Empirical absorption corrections were carried out using the DIFABS method.[29] Anisotropic thermal parameters were refined for all non-hydrogen atoms; hydrogen atoms were inserted in calculated positions (riding model). The final $wR(F^2)$ was 0.0438 $\{[\Sigma w(F_o^2 - F_c^2)/\Sigma w(F_o^2)^2]^{\frac{1}{2}}\}$, with conventional $R(F)$ 0.088 for the 237 parameters, using all data.

Atomic coordinates, thermal parameters, and bond lengths and angles have been deposited at the Cambridge Crystallographic Data Centre (CCDC). See Instructions for Authors, *J. Chem. Soc., Dalton Trans.*, 1997, Issue 1. Any request to the CCDC for this material should quote the full literature citation and the reference number 186/378.

Results

2,6-Bis[4-(*S*)-methyloxazolin-2-yl]pyridine

2,6-Bis[4-(*S*)-methyloxazolin-2-yl]pyridine (L) was prepared

Table 1 Analytical data for the complexes $[ReX(CO)_3L]$ and $[PtXMe_3L]$ (X = Cl, Br or I)

				Analysis[d] (%)		
Complex	Yield[a] (%)	$\tilde{\nu}(CO)$[b]/cm^{-1}	*m/z*[c]	C	H	N
$[ReCl(CO)_3L]$	20	1902, 1918, 2024	552, [*M* + H] 488, [*M* − Cl − CO]	35.0 (34.9)	2.75 (2.75)	7.65 (7.65)
$[ReBr(CO)_3L]$	21	1902, 1921, 2025	596, [*M* + H] 516, [*M* − Br]	33.9 (32.25)	2.55 (2.55)	7.4 (7.05)
$[ReI(CO)_3L]$	35	1903, 1923, 2025	644, [*M* + H] 516, [*M* − I]	29.9 (29.9)	2.5 (2.35)	6.45 (6.55)
$[PtClMe_3L]$	17		522, [*M* + H] 485, [*M* − Cl] 455, [*M* − Cl − 2Me]	33.6 (36.85)	4.55 (4.65)	6.95 (8.05)
$[PtBrMe_3L]$	42		485, [*M* − Br] 455, [*M* − Br − 2Me]	33.65 (35.9)	4.4 (4.5)	7.1 (7.85)
$[PtIMe_3L]$	40		612, [*M*] 485, [*M* − I] 455, [*M* − I − 2Me]	31.15 (31.4)	4.0 (3.95)	6.45 (6.85)

[a] Quoted relative to $[ReX(CO)_5]$ or $[(PtXMe_3)_4]$. [b] Recorded as CH_2Cl_2 solutions. [c] FAB mass spectral data. [d] Calculated values in parentheses.

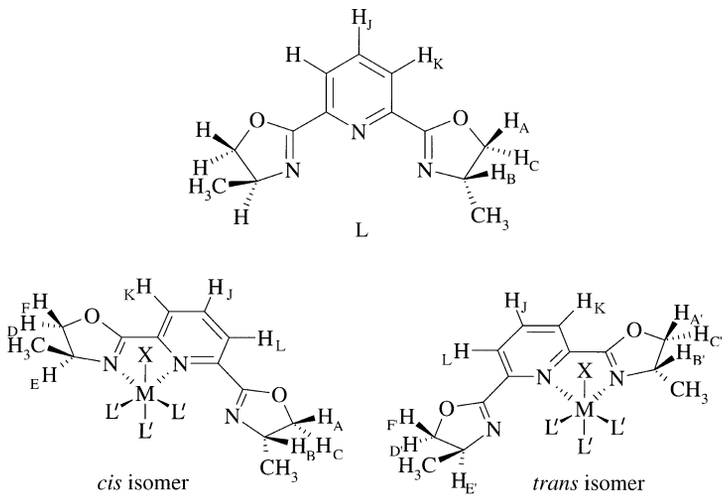

Scheme 2 2,6-Bis[4-(*S*)-methyloxazolin-2-yl]pyridine (L), and the *cis* and *trans* isomers of the complexes $[ReX(CO)_3L]$ and $[PtXMe_3L]$ (X = Cl, Br or I), showing the H atom labelling

Table 2 Hydrogen-1 NMR data[a] for 2,6-bis[4-(*S*)-methyloxazolin-2-yl]pyridine (L) and the complexes $[ReX(CO)_3L]$ (X = Cl, Br or I)

Compound	Isomer[b]	δ(oxazole CH_3)[c,d]	δ(oxazole H)[c]	Assignment[e]	δ(py H)[c]	Assignment[e]
Ligand		1.33 (6.7)	4.03 (≈8; [f] ≈8)	C	7.82 (7.9)	K
			4.0	B	8.13 (7.9)	J
			4.57 (≈8; [f] 9.5)	A		
$[ReCl(CO)_3L]$	Major (63)	1.40 (6.7) (maj, p)	4.06 (8.5)	C	7.94 (7.8)	K, L
	Minor (37)	1.40 (6.7) (min, p)	4.12 (8.6)	F′	8.07 (7.8)	J
		1.55 (6.5) (maj, c)	4.41 (8.7)	F		
		1.59 (6.6) (min, c)	4.56	B, B′, C′, E, E′		
			4.71 (9.0)	D′		
			4.78 (9.0)	A		
			4.94 (9.1)	A′		
			4.95 (9.1)	D		
$[ReBr(CO)_3L]$	Major (69)	1.40 (6.7) (min, p)	3.98 (8.1)	F′	7.93 (7.8)	K, L
	Minor (31)	1.40 (6.7) (maj, p)	4.05 (8.5)	C	8.06 (7.8)	J
		1.54 (6.6) (maj, c)	4.41 (8.6)	F		
		1.62 (6.6) (min, c)	4.56	B, B′, C′, E, E′		
			4.70 (9.0)	D′		
			4.78 (9.0)	A		
			4.95 (9.0)	A′		
			4.97 (9.2)	D		
$[ReI(CO)_3L]$	Major (74)	1.39 (≈7) (min, p)	4.05 (8.5)	C	7.91 (7.8)	L
	Minor (26)	1.41 (6.7) (maj, p)	4.11 (8.4)	F′	7.94 (7.8)	K
		1.55 (6.6) (maj, c)	4.42 (8.7)	F	8.05 (7.8)	J
		1.67 (6.6) (min, c)	4.58	B, B′, C′, E, E′		
			4.70 (8.9)	D′		
			4.79 (9.0)	A		
			4.96 (9.0)	A′		
			4.97 (9.2)	D		

[a] Recorded as $(CDCl_2)_2$ or $CDCl_3$ (see text) solutions at 298 K; chemical shifts quoted relative to $SiMe_4$ as an internal standard. [b] % Population in parentheses. [c] $^3J_{HH}$/Hz given in parentheses. [d] maj = Major isomers, min = minor isomer; p = pendant, c = co-ordinated. [e] See text and Scheme 2 for assignment. [f] $^2J_{HH}$/Hz.

by the same method as that previously described for the compound[15] 2,6-bis[4-(*S*)-isopropyloxazolin-2-yl]pyridine and the absolute configuration was confirmed by the crystal structure of the complex $[ReCl(CO)_3L]$ (see below). The assigment of the ^{1}H NMR spectrum of L is necessary before any assignment of the spectra of the complexes is possible (see below); a discussion of the ^{1}H NMR spectrum is therefore merited.

The ambient-temperature ^{1}H NMR spectrum (298 K, $CDCl_3$) of 2,6-bis[4-(*S*)-methyloxazolin-2-yl]pyridine displays signals in three regions. The two equivalent methyl groups of free L give rise to a doublet, due to coupling to H_B ($^3J_{HH}$ = 6.7 Hz) (see Scheme 2), at δ 1.33. The oxazole ring hydrogen nuclides give rise to three signals, in a 1:1:1 intensity ratio, in the region *ca.* δ 3.9–4.7. Proton H_B (Scheme 2) is easily distinguished by virtue of its complexity; it couples to the methyl group (see above) and to H_A and H_C, giving a complex multiplet of up to sixteen lines (not all of which are resolved). Protons H_A and H_C give rise to a doublet of doublets and a triplet. It is possible to distinguish between them by virtue of the different magnitudes of their vicinal scalar couplings to H_B. In planar five-membered rings (see above) *cis*-vicinal couplings are greater than *trans*-vicinal couplings;[30] thus the doublet of doublets ($^3J_{HH}$ = 9.5 Hz) is assigned to H_A, and the triplet ($^3J_{HH}$ ≈ 8 Hz) to H_C (Scheme 2). The ^4J scalar couplings between the oxazole methyl and H_A and H_C were not resolved. The aromatic region of the spectrum (*ca.* δ 7.7–8.2) displays a triplet (1 H) and a doublet (2 H) which are readily assigned to H_J and H_K, respectively. Hydrogen-1 NMR data are in Table 2.

Complexes $[ReX(CO)_3L]$

The three complexes $[ReX(CO)_3L]$ {X = Cl, Br or I; L = 2,6-

bis[4-(*S*)-methyloxazolin-2-yl]pyridine} were obtained as air-stable crystalline orange solids as described (see above). Their infrared spectra each displayed three bands in the carbonyl stretching region, characteristic of a *fac*-octahedral co-ordination geometry for the metal.[31] Fast atom bombardment (FAB) mass spectrometry was performed on samples of the complexes dissolved in a matrix of 3-nitrobenzyl alcohol. In each case strong peaks were observed for the species $[M + H]^+$; strong peaks corresponding to the loss of carbonyl groups and the halogen were also observed. Microanalyses for the complexes $[ReX(CO)_3L]$ (X = Cl or I) were consistent with the formation of analytically pure samples. The somewhat high carbon and nitrogen analyses obtained for the bromo complex, $[ReBr(CO)_3L]$, are thought to result from the presence of a minor product species, which was evidenced by (weak) extra signals in the ^{1}H NMR spectra. Analytical data are in Table 1.

NMR studies. The ambient-temperature (298 K) ^{1}H NMR spectra of the complexes $[ReX(CO)_3L]$ (X = Cl, Br or I), in $(CDCl_2)_2$ displayed well resolved signals due to the presence of two non-exchanging isomers in solution (see below). The spectra of all three complexes were similar, and the results obtained for the chloro-complex, $[ReCl(CO)_3L]$, will serve to illustrate the analysis of the problem.

The ^{1}H NMR spectrum of $[ReCl(CO)_3L]$ at 298 K displayed two sets of signals, with unequal intensities, owing to the presence of two solution-state isomers, labelled *cis* and *trans* according to the orientation of the co-ordinated oxazole-ring methyl group, with respect to the halogen (Scheme 2). The oxazole-ring methyl region displayed three doublets in a 1:1.7:2.7 intensity ratio, at δ 1.59, 1.55 and 1.40, respectively. The signal at δ 1.40 was presumed to result from overlap of the methyl signals of the pendant oxazole rings of both isomers, which would be expected to have very similar chemical shifts because they are remote from the site of co-ordination. The populations of the two solution-state isomers were determined by integration of the two highest-frequency oxazole-methyl doublets; the populations (X = Cl) are 37 and 63%. The assignment of the two isomers is problematical. The *cis* isomer may be expected to be disfavoured on steric grounds; chloride has a larger steric bulk than a carbonyl group. However, the *cis* isomer is present in the solid state [any steric interactions are clearly minimal (see below)], which *may* suggest that it is the dominant isomer in solution; the major solution-state species was therefore (tentatively) assigned to the *cis* isomer.

The unsymmetrical bidentate bonding mode of the ligand, L, renders all oxazole-ring hydrogen nuclides inequivalent; each of the two solution-state isomers therefore gives rise to six overlapping signals. The sets of signals due to the two isomers are readily distinguished by virtue of their different intensities. Furthermore, if it is assumed that the hydrogen nuclides of the co-ordinated oxazole rings resonate to higher frequency (as a consequence of their close proximity to the metal-co-ordinated N atom), then an assignment of the signals is possible by comparison with the spectrum of free L (see above). Thus the three triplets in the region *ca.* δ 4.0–4.45 were assigned to H_F, $H_{F'}$ and H_C (Scheme 2), respectively from high to low frequency. The complex multiplet centred at *ca.* δ 4.55 was assigned to the overlapping signals of $H_B/H_{B'}$, $H_E/H_{E'}$ and $H_{C'}$, and the four signals in the region *ca.* δ 4.6–5.1 were assigned to H_D, $H_{A'}$, H_A and $H_{D'}$, respectively from high to low frequency. A (^{1}H–^{1}H) correlation spectroscopy (COSY) experiment was also performed; the results obtained were entirely consistent with this assignment. The aromatic region of the ^{1}H NMR spectrum (*ca.* δ 7.55–8.15) displayed a doublet (2 H) and a triplet (1 H), due to H_K/H_L and H_J of the major isomer, respectively. The ^{1}H NMR spectrum of $[ReCl(CO)_3L]$ at 298 K is shown in Fig. 1.

On warming, reversible dynamic line broadening was observed in both the methyl and oxazole-H regions of the spectrum (see above). These band-shape changes indicated the onset of an exchange between the pendant and co-ordinated oxazole rings at a measurable rate on the NMR chemical shift timescale. The two solution-state isomers each give rise to a degenerate pair of species (Scheme 3); thus there are four species in solution, which must all be considered in the analysis of the dynamic NMR problem. The NMR line shapes of the methyl signals were submitted to a total band-shape analysis according to the dynamic Scheme 3, which causes an interconversion of the methyl groups according to the dynamic spin system (**I**).

The oxazole-methyl NMR line shapes were analysed on this basis. Attempts were made initially to simulate the band-shape changes to a single rate constant for: (*i*) a 'tick-tock twist' mech-

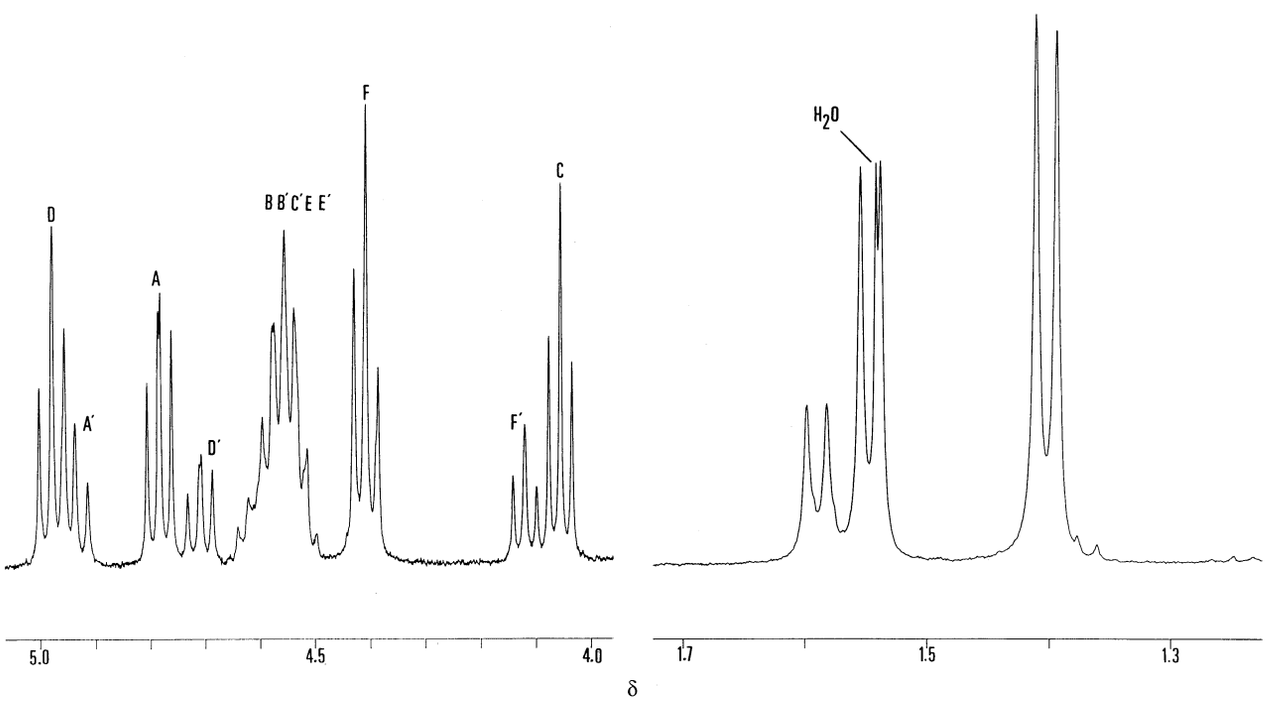

Fig. 1 The 400 MHz ^{1}H NMR spectrum of $[ReCl(CO)_3L]$ at 303 K, showing the oxazole-Me and -H regions. See Scheme 2 for labelling

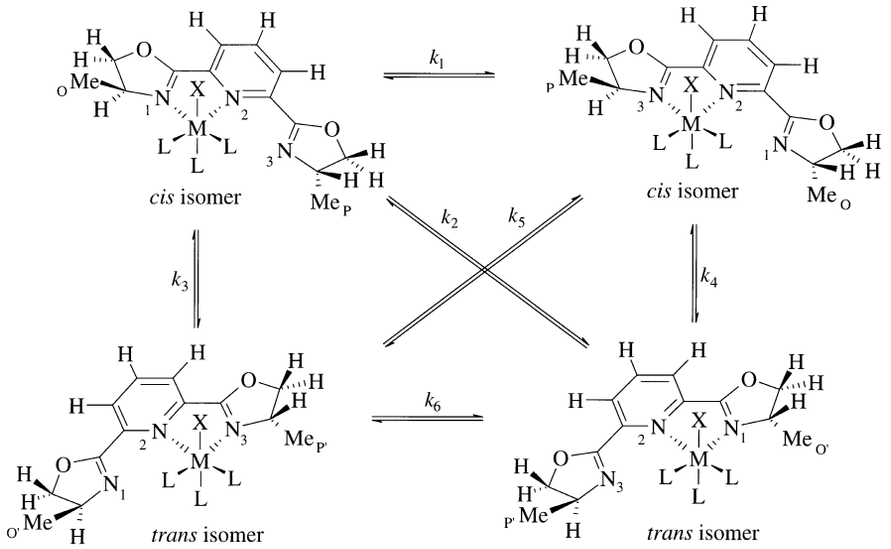

Scheme 3 The four solution-state species of the complexes [ReX(CO)$_3$L] and [PtXMe$_3$L] (X = Cl, Br or I), showing the possible interconversion pathways between them. Note that $k_1 = k_6$, $k_3 = k_4$ and $k_2 = k_5$, giving three possible *independent* rate processes

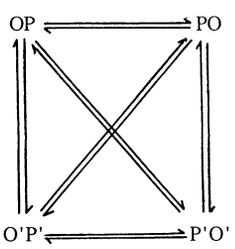

I

anistic pathway [*i.e.* k_3 (= k_4) only, with all other rates assumed to be negligible] (Scheme 3); (*ii*) a 'rotation' mechanistic pathway [*i.e.* k_1 (= k_6) only, again all other rates assumed to be negligible] (Scheme 3); (*iii*) a ligand-dissociation pathway (*i.e.* $k_1 = k_2 = k_3 = k_4 = k_5 = k_6$). However, the experimental spectra could not be simulated on the basis of a single rate process. Accurate fits between the experimental and computer-simulated spectra could only be obtained when two *independent* rate constants were used, *viz.* k_1 (k_6) and k_3 (k_4) (see above). At probe temperatures above *ca.* 380 K appreciable decomposition of the complex occurred, and it was not possible accurately to simulate the dynamic NMR spectra above this temperature; however, twelve reliable fits were obtained, five of which are shown in Fig. 2. The Eyring and Arrhenius activation parameters determined for the complexes [ReX(CO)$_3$L] (X = Cl, Br or I) are in Table 3.

In the tricarbonylhalogenorhenium(I) complexes of 2,2′:6′,2″-terpyridine, [ReX(CO)$_3$(terpy)] (X = Cl, Br or I),[3] restricted rotation of the pendant pyridyl ring was observed by low-temperature dynamic NMR studies. A corresponding study of the complex [ReCl(CO)$_3$L] was therefore carried out in CD_2Cl_2, in order to study any restricted rotation of the pendant oxazole ring. However no evidence of any restricted rotation about the C (pyridyl)–C (pendant oxazole) bond was observed, even at temperatures below 193 K. It is possible that the rotation of the pendant oxazole ring is rapid on the NMR timescale at these low temperatures; however, it is thought more likely that the complex exists in one highly dominant rotomeric form, making the NMR line shapes insensitive to any restricted rotation.

Crystal structure of [ReCl(CO)$_3$L]. The crystal structure of [ReCl(CO)$_3$L] was determined primarily to confirm the bidentate bonding mode of the ligand, 2,6-bis[4-(*S*)-methyloxazolin-2-yl]pyridine and its absolute configuration. A view of the mol-

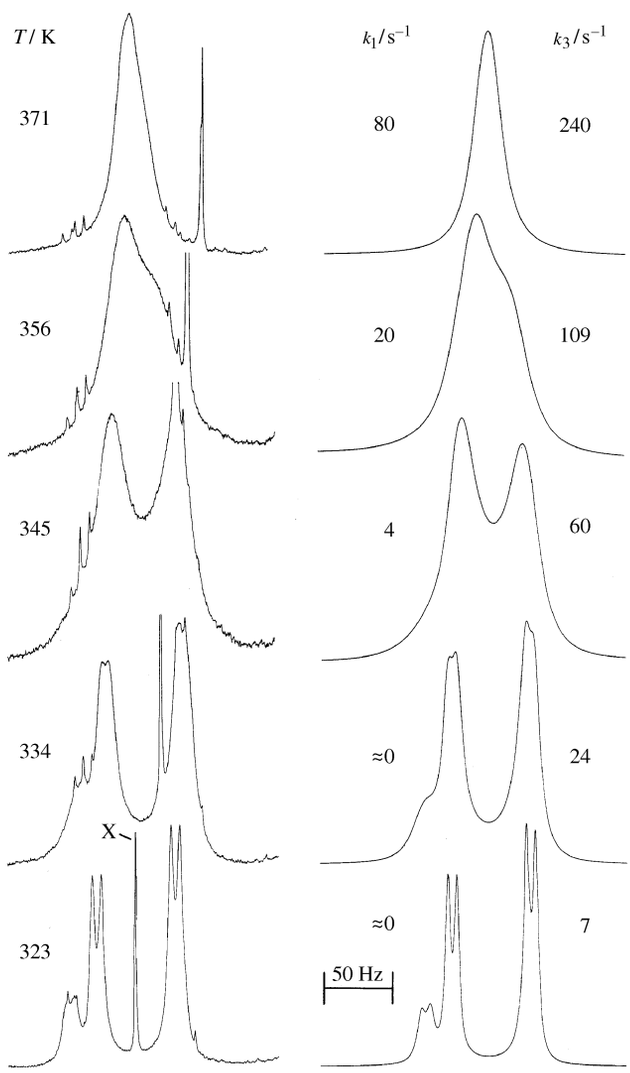

Fig. 2 Variable-temperature ^{1}H NMR spectra of [ReCl(CO)$_3$L]. 'Best-fit' computer-simulated spectra are shown alongside, with the rate constants k_1 and k_3 (see Scheme 3) for the two independent exchange pathways. 'Best-fit' rate constants (s^{-1}), k_1 and k_3, for the other temperatures are as follows: 0, 1.1 (313); 0, 13 (328); 0, 34 (339); 12, 84 (350); 35, 144 (361); 54, 184 (366) and 130, 291 (377 K). The signal X, which moves appreciably, is probably due to water

Table 3 Activation parameters[a] for the complexes $[ReX(CO)_3L]$ (X = Cl, Br or I)

Complex	Mechanism[b]	E_a/kJ mol^{-1}	log (A/s^{-1})	$\Delta H^{\ddagger}$/kJ mol^{-1}	$\Delta S^{\ddagger}$/J K^{-1} mol^{-1}	$\Delta G^{\ddagger}$/kJ mol^{-1}
$[ReCl(CO)_3L]$	Tick-tock twist[c]	79.7 (5.5)	13.7 (0.8)	76.9 (5.6)	7.8 (16.1)	74.5 (0.8)
	Rotation	111.6 (7.7)	17.6 (1.1)	108.6 (7.7)	82.7 (21.5)	83.9 (1.3)
$[ReBr(CO)_3L]$	Tick-tock twist[c]	77.4 (3.6)	13.3 (0.5)	74.5 (3.6)	−0.4 (10.4)	74.7 (0.5)
	Rotation	84.9 (6.9)	13.8 (1.0)	81.9 (6.9)	9.4 (19.2)	79.1 (1.2)
$[ReI(CO)_3L]$	Tick-tock twist[c]	68.8 (5.3)	11.9 (0.8)	66.0 (5.3)	−25.6 (15.6)	73.6 (0.6)
	Rotation	134.7 (8.4)	20.8 (1.3)	131.8 (8.4)	143.6 (23.9)	89.0 (1.2)

[a] Errors given in parentheses; $\Delta G^{\ddagger}$ quoted at 298 K. [b] See Scheme 1 for mechanism. [c] Data refer to the process major isomer ⟶ minor isomer.

Table 4 Selected bond lengths (Å) and angles (°) for the complex $[ReCl(CO)_3L]$

Re–C(14)	1.903(14)	C(1)–C(2)	1.53(2)
Re–C(15)	1.89(2)	C(2)–C(3)	1.59(2)
Re–C(16)	1.93(2)	O(1)–C(3)	1.472(14)
Re–N(1)	2.140(10)	O(1)–C(4)	1.346(13)
Re–N(2)	2.256(9)	N(1)–C(4)	1.256(12)
Re–Cl	2.485(3)	C(4)–C(5)	1.45(2)
N(1)–C(2)	1.46(2)	N(3)–C(10)	1.27(2)
N(1)–Re–N(2)	74.7(3)	Cl–Re–C(16)	176.6(4)
N(1)–Re–C(14)	94.3(5)	C(2)–N(1)–C(4)	108.5(10)
N(1)–Re–C(15)	174.2(4)	N(1)–C(2)–C(3)	103.1(9)
N(1)–Re–C(16)	97.8(4)	C(2)–C(3)–O(1)	102.6(10)
N(1)–Re–Cl	83.1(2)	C(3)–O(1)–C(4)	106.1(9)
N(2)–Re–Cl	83.8(2)	C(1)–C(2)–C(3)	114.5(11)
N(2)–Re–C(15)	102.9(4)	C(1)–C(2)–N(1)	111.7(10)
N(2)–Re–C(16)	97.8(4)	N(1)–C(4)–O(1)	119.2(10)
C(14)–Re–C(15)	87.9(5)	N(2)–C(5)–C(6)	121.6(11)

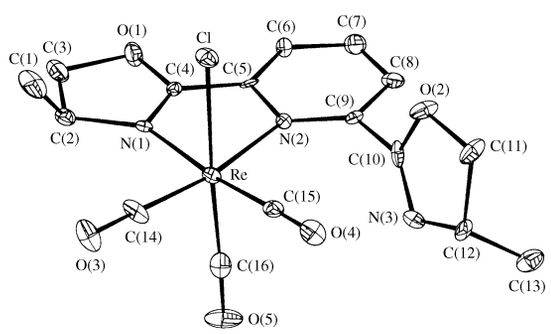

Fig. 3 Crystal structure of $[ReCl(CO)_3L]$, showing the atom labelling scheme

ecule, indicating the atom numbering scheme, is shown in Fig. 3. This clearly reveals the expected *fac*-octahedral co-ordination geometry of the metal, and the bidentate bonding mode of the ligand. The absolute configuration (*S*) of the ligand is also confirmed. Selected bond lengths and angles are in Table 4.

Examination of the bond angles reveals that the metal environment deviates somewhat from an idealised octahedral geometry; this is due principally to the small bite size of the ligand {N(1)–Re–N(2) 74.7(3)°, *cf.* 74.3(4)° for $[ReBr(CO)_3(terpy)]$[3]}. Both of the oxazole rings are essentially planar, and the pendant ring is rotated with respect to the plane containing N(1), Re and N(2) [dihedral angle = 76.2(4)°] (see Fig. 3). It is also interesting that the methyl group of the co-ordinated oxazole ring is oriented *cis* to the chloride. The C(1)···Cl non-bonding distance is 3.583(5) Å [*cf.* $C(1)H_{calc}\cdots Cl$ *ca.* 3.63 Å], which is comparable to the sum of the van der Waals radii[32] (3.66 Å) for chlorine and carbon; thus any steric interactions are minimal. The Re–N(1) (oxazole) distance [2.140(10) Å] is relatively short [*cf.* Re–N(2) (pyridyl) 2.256(9) Å] and indicates the formation of a strong Re–N (oxazole) bond.

Complexes $[PtXMe_3L]$

The three complexes $[PtXMe_3L]$ {X = Cl, Br or I; L = 2,6-bis[4-(*S*)-methyloxazolin-2-yl]pyridine} were prepared as air-stable cream-white solids as described (see above). They proved difficult to purify and as a result poor analytical figures were obtained. However, the FAB mass spectrometry data were consistent with the presence of the formulated species. Analytical data are in Table 1.

NMR studies. The ambient-temperature (298 K) ^{1}H NMR spectra of the complexes $[PtXMe_3L]$ (X = Cl, Br or I) in $CDCl_3$ solution displayed signals in three regions: (*i*) the methyl region (*ca.* δ 0.5–2.0), (*ii*) the oxazole-H region (*ca.* δ 2.8–5.2) and (*iii*) the aromatic region (*ca.* δ 7.8–8.2). The oxazole-H and the aromatic regions of the spectra were exactly analogous to the spectra of the rhenium(I) complexes, $[ReX(CO)_3L]$ (see above). However, the chemical shift differences between the oxazole-H atom signals were generally small and an unambiguous assignment of this region was not possible.

The methyl region of the spectra was highly complex, owing to the presence of six methylplatinum signals (three due to each of the two solution-state isomers), with ^{195}Pt satellites (33% abundance, $I = \frac{1}{2}$), in addition to the four oxazole-Me doublets (see above). Despite the complexity of the spectra in this region, a full assignment of the oxazole- and platinum-methyl signals was possible for the bromo- and iodo-complexes. The signals due to the two isomers were readily distinguished by virtue of their different intensities. The oxazole-Me group signals were assigned on the same basis as that described for the rhenium(I) complexes, $[ReX(CO)_3L]$. In the case of the chloro complex, $[PtClMe_3L]$, there was considerable overlap of the signals and an unambiguous assignment was not feasible. The methyl region of the ^{1}H NMR spectrum of $[PtBrMe_3L]$ is shown in Fig. 4. Hydrogen-1 NMR data are in Table 5.

On warming, reversible dynamic NMR line broadening was observed in both the oxazole-H and methyl regions of the ^{1}H NMR spectra of the complexes, indicating the onset of the expected structural rearrangement at a measurable rate on the NMR chemical shift time-scale. The complex band-shape changes observed in the methyl region were further complicated by the onset of platinum–methyl scrambling[33] at elevated temperatures, which frustrated attempts accurately to simulate the variable-temperature spectra. The ^{195}Pt NMR spectra of the complexes were therefore investigated.

As expected, the ambient temperature [303 K, $(CDCl_2)_2$] ^{195}Pt NMR spectra of the three complexes, $[PtXMe_3L]$ (X = Cl, Br or I), each displayed two bands (see Fig. 5), due to the two solution-state isomers (Scheme 2); the populations of the isomers (Table 5) were determined by integration of the two ^{195}Pt NMR signals. On warming, these bands broadened, coalesced and eventually sharpened to give a single peak (see Fig. 5). As in the analogous rhenium(I) complexes (see above), each isomer consists of a pair of degenerate species (Scheme 3); however, the ^{195}Pt NMR spectra are insensitive to the exchange of these degenerate species [which occurs *via* the rotation mechanism (see Schemes 1 and 3)]. Thus the observed band-shape changes must result from either the 'tick-tock twist' pathway for the fluxional rearrangement or from ligand dissociation (or a combination of both). It is not possible to distinguish between these possibilities; however, if the platinum complexes behave in a similar manner to the rhenium(I) complexes (as would be

Table 5 Hydrogen-1 and ^{195}Pt NMR data[a,b] for the complexes [PtXMe$_3$L] (X = Cl, Br or I)

Complex	Isomer	Population (%)[b]	δ(Pt–CH$_3$)[c]	δ(oxazole CH$_3$)[d]	δ(^{195}Pt)
[PtClMe$_3$L]	Major	67	*e*	*e*	2060.7
	Minor	33			2058.1
[PtBrMe$_3$L]	Major	70	1.01 (75.2)	1.38 (7.1) (p)	2049.0
			1.17 (72.8)	1.43 (6.6) (c)	
			1.53 (78.9)		
	Minor	30	0.71 (73.3)	1.36 (6.0) (p)	2040.4
			1.18 (72.9)	1.59 (6.6) (c)	
			1.55 (79.4)		
[PtIMe$_3$L]	Major	69	1.14 (73.3)	1.45 (6.6) (p)	1869.2
			1.39 (73.7)	1.51 (6.6) (c)	
			1.75 (79.2)		
	Minor	31	0.87 (71.6)	1.44 (6.5) (p)	1846.1
			1.39 (73.7)	1.73 (6.6) (c)	
			1.74 (79.4)		

[a] Proton NMR spectra recorded at 298 K in $CDCl_3$, chemical shifts quoted relative to $SiMe_4$ as an internal standard; ^{195}Pt NMR spectra recorded at 303 K in $(CDCl_2)_2$, chemical shifts quoted relative to Ξ(^{195}Pt) = 21.4 MHz. [b] Isomer populations determined by integration of ^{195}Pt NMR signals. [c] $^2J_{PtH}$/Hz in parentheses. [d] $^3J_{HH}$/Hz in parentheses; p = pendant, c = co-ordinated. [e] Data not measured (see text).

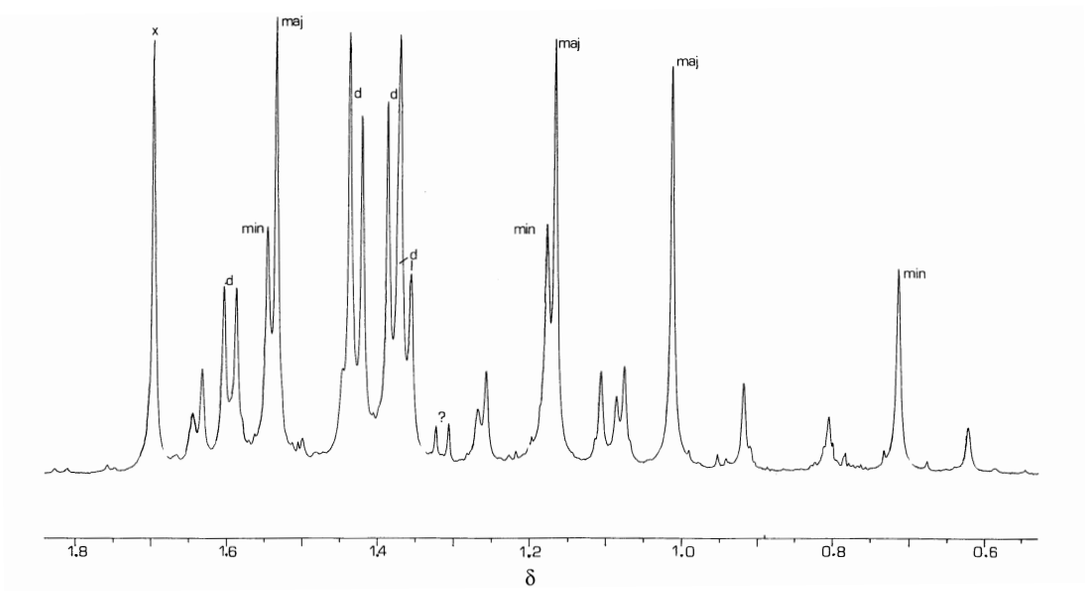

Fig. 4 The 400 MHz ^{1}H NMR spectrum of [PtBrMe$_3$L) at 303 K, showing the oxazole- and platinum-methyl region. The four oxazole-Me doublets are labelled d; min = minor isomer, maj = major isomer. Impurity is denoted ? The signal X is probably due to water

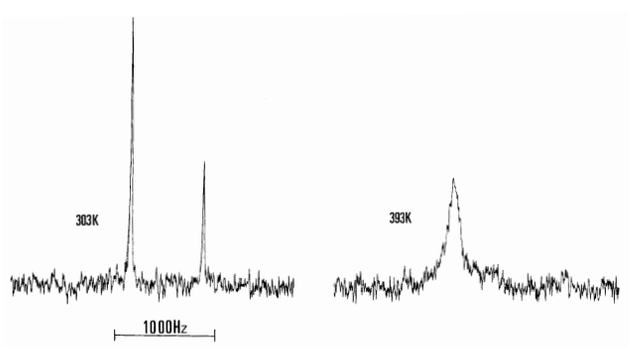

Fig. 5 Platinum-195 NMR spectra of [PtBrMe$_3$L] at 303 and 393 K

expected), then the line-shape changes presumably result entirely from a 'tick-tock twist' mechanistic process (at least at moderate temperatures). Unfortunately, the determination of reliable quantitative kinetc data for the rearrangement was not possible because of insufficient quantities of the samples to acquire good-quality ^{195}Pt NMR spectra over a wide temperature range (particularly near coalescence).

Discussion

The possible mechanisms of the 1,4-metal–ligand rearrangements observed in analogous complexes to those reported here have been described in some detail,[2–11] and are depicted in Scheme 1. The two rearrangement pathways are, in principle, distinguishable by virtue of their different effects on the equatorial ligands of the metal moiety; mechanism (i) ('rotation') does not lead to an exchange of equatorial environments, whereas, (ii) ('tick-tock twist') does. Studies on the platinum(IV) complexes, [PtXMe$_3$L] (X = Cl, Br or I; L = potentially terdentate ligand acting in a bidentate bonding mode), indicated that the so called 'tick-tock twist' mechanism [(ii) in Scheme 1] was occurring; the equatorial PtMe groups were exchanged during the rearrangement.

The use of (enantiomerically pure) chiral ligands enables the mechanism to be monitored by the changes in the dynamic NMR band shapes of the ligand; the two mechanisms proposed previously (see above) can be readily distinguished by their different effects on the oxazole-methyl signals. If a 'rotation' mechanism is occurring then the pendant and co-ordinated oxazole rings of each isomer are exchanged, but isomers are not (Scheme 3); thus in the fast-exchange limit two methyl doublets of unequal intensity would be expected. Conversely, if a 'tick-tock twist' mechanism is occurring, isomers are exchanged, but pendant and co-ordinated oxazole rings *within each isomer* are not; thus in the fast-exchange limit, two methyl doublets of equal intensity would be expected. However, it was evident from

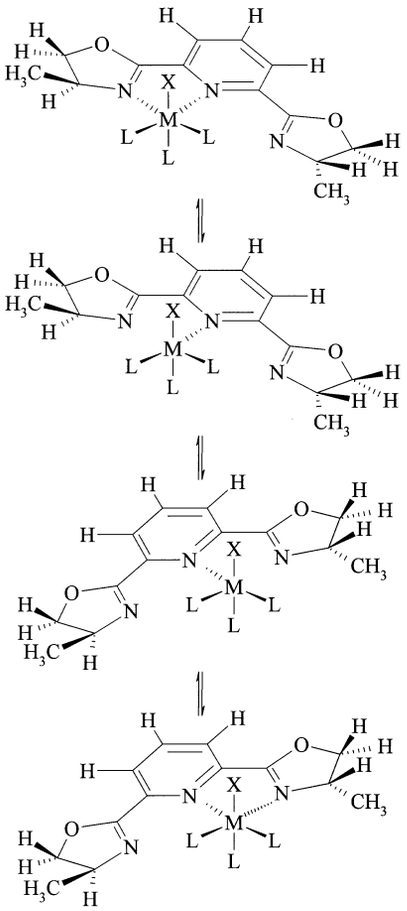

Scheme 4 A third possible mechanism for the fluxional rearrangement observed in the complexes [ReX(CO)$_3$L] and [PtXMe$_3$L] (X = Cl, Br or I)

the simulation of the experimental variable-temperature ^{1}H NMR spectra (see above) that both of these mechanisms were occurring; the band-shape changes could only be simulated when non-zero rate constants were used for k_3 (k_4) *and* k_1 (k_6) (Scheme 3). A third possible mechanism (depicted in Scheme 4), analogous to that proposed by Rotondo *et al.*[7] for the square-planar complexes *cis*-[M(C$_6$F$_5$)$_2$(terpy)] (M = Pd or Pt), cannot be ruled out entirely. However, this mechanism is considered unlikely because in the five-co-ordinate transition state free rotation about the Re–N (pyridyl) bond would be expected, which would facilitate the exchange pathway k_2 (k_5), shown in Scheme 3; the dynamic NMR line shapes cannot be simulated when non-zero magnitudes for k_2 (k_5) are employed.

Examination of the magnitudes of the free energies of activation, $\Delta G^{\ddagger}$ (298 K) (Table 3), obtained for the complexes [ReX(CO)$_3$L] (X = Cl, Br or I) reveal several points.

(*i*) The activation energies for the 'rotation' pathway are (on average) *ca.* 10 kJ mol^{-1} higher than for the 'tick-tock twist' pathway. This increase in $\Delta G^{\ddagger}$ presumably arises because, for the 'rotation' mechanism to occur, complete cleavage of the Re–N (oxazole) bond is necessary, whereas in the 'tick-tock twist' mechanism there is only partial cleavage (*i.e.* a lengthening) of the bond, concomitant with the formation of a pseudo-terdentate transition state.

(*ii*) The nature of the halogen appears to have only a small effect on the magnitude of $\Delta G^{\ddagger}$ for the 'tick-tock twist'. This is to be expected because the halide has a *cis* relationship to the fluxional Re–N bonds. Conversely, the halogen appears to have a large effect on the magnitude of the free energy of activation for the 'rotation' pathway. This is difficult to rationalise. The activation entropies, $\Delta S^{\ddagger}$, for the 'tick-tock twist' and the 'rotation' are also noteworthy. Although activation entropies are subject to large errors (particularly over narrow temperature ranges) and should be viewed with caution, it is clear that for the 'tick-tock twist', $\Delta S^{\ddagger}$(average) is negative (−6.1 J K^{-1} mol^{-1}), whereas for the 'rotation' it is positive (+78.6 J K^{-1} mol^{-1}). This is in line with the proposed transition states for the two mechanisms; the 'tick-tock twist' transition state is considerably more ordered than that of the 'rotation' mechanism (see Scheme 1).

(*iii*) The free energies of activation for the complexes [ReX(CO)$_3$L] {X = Cl, Br or I; L = 2,6-bis[4-(*S*)-methyloxazolin-2-yl]pyridine} are the highest reported thus far for a 1,4-Re–N fluxional shift of this type (see ref. 9). This may be as a result of either a stabilisation of the ground state or a destabilisation of the transition state. It is not possible to distinguish between these two possibilities by dynamic NMR methods; however, it is believed that the large magnitudes of $\Delta G^{\ddagger}$ stem primarily from stabilisation of the ground state, as a result of the formation of a strong Re–N (oxazole) bond (see above).

Conclusion

The use of single-enantiomer chiral ligands as a mechanistic probe for dynamic structural rearrangements in organo-transition-metal complexes has been demonstrated. This work has shown that the fluxional rearrangement observed in bidentate complexes of the potentially terdentate ligand, 2,6-bis[4-(*S*)-methyloxazolin-2-yl]pyridine occurs *via* both 'tick-tock twist' and 'rotation' mechanisms. The results of further studies into the fluxional behaviour of 'chiral-at-ligand' organometallic complexes will be published shortly.

Acknowledgements

We are grateful to the University of Wales, Swansea for financial support, and to Miss Tina Einfeld and Mr. Peter Haley for some preliminary synthetic work. Professor M. B. Hursthouse and Mr. D. E. Hibbs are acknowledged for the collection of the X-ray data.

References

1 E. C. Constable, *Adv. Inorg. Chem. Radiochem.*, 1987, **30**, 69.
2 E. W. Abel, V. S. Dimitrov, N. J. Long, K. G. Orrell, A. G. Osborne, H. M. Pain, V. Sik, M. B. Hursthouse and M. A. Mazid, *J. Chem. Soc., Dalton Trans.*, 1993, 291.
3 E. W. Abel, V. S. Dimitrov, N. J. Long, K. G. Orrell, A. G. Osborne, H. M. Pain, V. Sik, M. B. Hursthouse and M. A. Mazid, *J. Chem. Soc., Dalton Trans.*, 1993, 597.
4 E. R. Civitello, P. J. Dragovich, T. B. Karpishin, S. G. Novick, G. Bierach, J. F. O'Connel and T. D. Westmoreland, *Inorg. Chem.*, 1993, **32**, 237.
5 E. W. Abel, K. G. Orrell, A. G. Osborne, H. M. Pain and V. Sik, *J. Chem. Soc., Dalton Trans.*, 1994, 111.
6 (*a*) E. W. Abel, K. G. Orrell, A. G. Osborne, H. M. Pain, V. Sik, M. B. Hursthouse and K. M. A. Malik, *J. Chem. Soc., Dalton Trans.*, 1994, 3441; (*b*) E. W. Abel, A. Gelling, K. G. Orrell, A. G. Osborne and V. Sik, *Chem. Commun.*, 1996, 2329.
7 E. Rotondo, G. Giordano and D. Minniti, *J. Chem. Soc., Dalton Trans.*, 1996, 253.
8 E. W. Abel, K. A. Hylands, M. D. Olsen, K. G. Orrell, A. G. Osborne, V. Sik and G. N. Ward, *J. Chem. Soc., Dalton Trans.*, 1994, 1079.
9 A. Gelling, K. G. Orrell, A. G. Osborne and V. Sik, *J. Chem. Soc., Dalton Trans.*, 1994, 3545.
10 E. W. Abel, D. Ellis and K. G. Orrell, *J. Chem. Soc., Dalton Trans.*, 1992, 2243.
11 E. W. Abel, P. J. Heard, K. G. Orrell, M. B. Hursthouse and M. A. Mazid, *J. Chem. Soc., Dalton Trans.*, 1993, 3795.
12 E. W. Abel, D. Ellis, K. G. Orrell and V. Sik, *Polyhedron*, 1991, **10**, 1063.
13 E. W. Abel, J. C. Domer, D. Ellis, K. G. Orrell, V. Sik, M. B. Hursthouse and M. A. Mazid, *J. Chem. Soc., Dalton Trans.*, 1992, 1073.
14 R. Romeo, A. Grassi and L. M. Scolaro, *Inorg. Chem.*, 1992, **31**, 4383.
15 H. Nishiyama, M. Kondo, T. Nakamura and K. Itoh, *Organometallics*, 1991, **10**, 580.

16 T. G. Grant and A. I. Meyers, *Tetrahedron*, 1994, **50**, 2297 and refs. therein.
17 S. P. Schmidt, W. C. Trogler and F. Basolo, *Inorg. Synth.*, 1979, **28**, 160.
18 J. C. Baldwin and W. C. Kaska, *Inorg. Chem.*, 1975, **14**, 2020.
19 D. H. Goldsworthy, Ph.D. Thesis, University of Exeter, 1980.
20 D. F. Shriver, *Manipulation of Air-sensitive Compounds*, McGraw-Hill, New York, 1969.
21 D. D. Perrin and W. L. F. Armarego, *Purification of Laboratory Chemicals*, Pergamon, Oxford, 1988.
22 D. A. Kleier and G. Binsch, DNMR 3, Quantum Chemistry Exchange, Indiana University, 1970.
23 G. Binsch and H. Kessler, *Angew. Chem., Int. Ed. Engl.*, 1980, **19**, 411.
24 G. Bodenhausen, H. Kogler and R. R. Ernst, *J. Magn. Reson.*, 1984, **58**, 370.
25 J. A. Darr, S. R. Drake, M. B. Hursthouse and K. M. A. Malik, *Inorg. Chem.*, 1993, **32**, 5704.
26 G. M. Sheldrick, *Acta Crystallogr., Sect. A*, 1990, **46**, 467.
27 G. M. Sheldrick, SHELXL 93, Program for Crystal Structure Refinement, University of Göttingen, 1993.
28 J. A. Ibers and W. C. Hamilton (Editors), *International Tables for X-Ray Crystallography*, Kynoch Press, Birmingham, 1974, vol. 4.
29 N. P. C. Walker and D. Stuart, *Acta Crystallogr., Sect. A*, 1983, **39**, 158; adapted for FAST geometry by A. I. Karavolv, University of Wales, Cardiff, 1991.
30 R. J. Abraham, J. Fisher and P. Loftus, *Introduction to NMR Spectroscopy*, Wiley, New York, 1991.
31 D. A. Edwards and J. Marshalsea, *J. Organomet. Chem.*, 1977, **131**, 73.
32 J. Emsley, *The Elements*, Oxford University Press, 2nd edn., 1991.
33 E. W. Abel, S. K. Bhargava and K. G. Orrell, *Prog. Inorg. Chem.*, 1984, **32**, 1.

Received 5*th September* 1996; *Paper* 6/06109E